Journal of Machine Engineering, 2024, Vol. 24, No. 3, 75–94
ISSN 1895-7595 (Print) ISSN 2391-8071 (Online)

Received*: 30 March 2024* / Accepted: *15 July 2024* / Published online: *30 August 2024*

shrink-fit, ultrasonic, strength enhancement, FCCCD method

Loc Huu NGUYEN[1,2*],
Phong Vi LAM[1,2.]

EFFECTS OF ULTRASONIC OSCILLATION ON SHRINK-FITTED ASSEMBLY

Shrink-fitting is widely recognized as the primary method for assembling interference fits. However, the use of the shrink-fitting technique in forming linkages between parts is often constrained by the requirement for high temperatures and the inevitable occurrence of surface damage. Consequently, an analysis of the integration of high-frequency stimulation, also known as ultrasonic oscillation, has been undertaken to develop a novel assembly procedure aiming at reducing the issues associated with shrink-fitted joints. The oscillation was conducted with generating power ranging from 500 W to 1500 W and processing time from 10 to 70 seconds. The ultrasonic oscillated shrink-fitting procedure exhibits significant advantages, reduces surface damage while concurrently enhancing the axial holding load limit of the joint. This approach opens the door to the integration of new assembly techniques in small mechanisms, where straightforward joints are of paramount importance.

1. INTRODUCTION

Interference fit typically involves the assembly of two parts directly connected without the need for auxiliary mechanisms. One common instance of an interference fit occurs between cylindrical components, such as shafts and hubs, where the hub's actual diameter is intentionally smaller than the shaft's actual diameter. This diameter difference constitutes the primary characteristic of an interference fit, often referred to as the interference value, which significantly impacts the overall load capacity of the fit [1]. Interference fits play a vital role in enhancing the reliability, performance, and automation potential of mechanical systems.

Two main assembly processes, press-fitting (PF) and shrink-fitting (SF), are considered in this context. PF involves bringing the parts together through axial loading, commonly performed using hydraulic systems. In contrast, SF relies on the thermal expansion or contraction behaviour of materials. Typically, for SF, the hub is heated to induce a controlled expansion, creating a micro gap with the shaft, which is then inserted into the hub. In cases where heating the hub is not feasible, the shaft can be cooled using liquid nitrogen or liquid carbon dioxide. Moreover, for more demanding interference fits with significant interference values, a combination of hub heating and shaft cooling may be employed simultaneously [2].

[1] Department of Machine Design, Ho Chi Minh City University of Technology (HCMUT), Vietnam
[2] Vietnam National University Ho Chi Minh City, Linh Trung Ward, Thu Duc City, Vietnam
[*] E-mail: nhloc@hcmut.edu.vn
https://doi.org/10.36897/jme/190105

While these conventional assembly methods have been broadly used for decades, they come with inherent drawbacks. PF consumes substantial energy and carries a high risk of negatively impacting the surface of the assembled parts. On the other hand, SF can be problematic for materials sensitive to temperature changes, potentially affecting material properties and overall part structure [3]. Consequently, recent research has focused on overcoming these limitations by optimizing assembly parameters and even developing innovative assembly processes.

Since the early 1950s, the utilization of high-frequency vibration, commonly referred to as ultrasonic oscillation, has been the subject of research concerning material behaviour, particularly focusing on the plastic deformation of materials. Building upon these foundational insights, novel manufacturing processes have emerged, specifically ultrasonic-assisted forming techniques [4], with the most significant outcomes being the reduction of required forces, attributed to decreased sliding friction [5]. These processes operate within the realm of stress superposition, acoustic softening, and other acoustic phenomena inherent in the microstructure of materials [6, 7].

Despite the favourable outcomes observed in these studies, it is worth noting that they predominantly investigate plastic deformation in materials. However, this state represents only one facet of the diverse material behaviours encountered in mechanical applications. Consequently, this research gap prompts exploration into the effects of vibration in other material states, such as elastic deformation, which, despite its expanding applications, has received limited attention [8], particularly in the realm of interference-fitting involving elastic-plastic deformation [9].

In light of these intriguing mechanisms associated with ultrasonic oscillation, numerous research endeavours and analyses have begun to explore the advantages and assisting capabilities of this type of vibration in interference fits, yielding promising results. Previous studies primarily concentrated on press fits, asserting a significant reduction in assembly and disassembly forces through the application of high-frequency vibration. Different oscillation parameters were found to produce distinct outcomes. Notably, oscillation demonstrated a diminishing effect on load capacity, suggesting evidence of friction reduction and surface modification [10–13].

These noteworthy findings laid the groundwork for subsequent researchers to delve into the utilization of ultrasonic oscillation for connecting electrical components. They confirmed that only 20% of the normal assembly force requirement was necessary compared to conventional PF without vibration. Furthermore, this analysis revealed that different vibrational inputs allowed for relative control over component deformation, enabling the mass installation of a substantial number of components with minimal force and a reduced risk of component failure [14].

Existing research on interference fits encompasses a range of vibration frequencies, spanning from low frequencies of around 40 Hz and 120 Hz [10, 13] to high frequencies such as 20 kHz, 40 kHz [11, 12], and even extremely high frequencies between 250 kHz and 500 kHz [14] (as listed in Table. 1). However, the majority of previous studies have primarily concentrated on PF scenarios, where the impact of vibrational stimulation occurs during the assembly process, particularly within the context of asperities flattening. The observed outcomes have revealed a reduction in load requirements and significant surface damage.

Furthermore, the scope of these relevant studies exploring high-frequency and extremely high-frequency vibrations has been predominantly limited to mini/micro assembly processes within the field of electrical applications. In contrast, when it comes to characterizing interference fits involving larger diameter ranges, typical of conventional mechanical fits, the current state of research primarily focuses on lower frequencies ranging from 20 Hz to 120 Hz. Additionally, the materials considered in these cases often represent plastic samples utilized solely for experimental purposes [10]. Given this research landscape, there exists a critical need for further investigations that delve into the effects of ultrasonic oscillation within the context of interference fits.

Table 1. Comparison of various related research

Article	Oscillation frequency range	Nominal diameter range	Contact case
Effects of ultrasonic oscillation on shrink-fitted assembly (our research)	High-frequency 20 kHz	Conventional fit 20 mm	Shrink-fitting
Elastic-plastic cube model for ultrasonic friction reduction via Poisson's effect [8]	Low-frequency 40–120 Hz	Conventional fit 30 mm	Press-fitting
Experimental investigation of interference fit connection of mechanical components [10]	High-frequency 40 kHz	Miniaturized fit 997–1020 μm	Press-fitting
Ultrasonic press-fitting: A new assembly technique [11]	High-frequency 18.2 kHz	Conventional fit 6 mm	Press-fitting
Ultrasonic assembly of press-fit joints [12]	Low-frequency 42 Hz	Conventional fit 4–12 mm	Press-fitting
A study on the experimental investigation of low frequency vibration wave assisted disassembly of press-fit joints [13]	Extremely high-frequency 250–500 kHz	Micro fit	Press-fitting

The information presented above serves as the foundational basis for the objectives of this research. Initially, the focus of this study was directed towards investigating the scenario of SF as opposed to PF. In this approach, the effects of ultrasonic oscillation were introduced after the assembly process. This methodology was adopted to consider additional influences beyond force reduction, recognizing that the primary aim of an interference fit is to withstand the required load and ideally maximize it.

The selected frequency level was established at 20 kHz, a common parameter in various ultrasonic generating systems. Through the utilization of the face-centered central composite design (FCCCD) response surface method, this study also determined the optimal parameters for oscillating time and generating power to achieve the highest load capacity. Furthermore, this experimental investigation involved comprehensive observations through surface profiling and microscopic imaging. These observations were undertaken with a specific focus on elucidating the effects of ultrasonic oscillation within the framework of conventional

interference fits, with particular emphasis on the SF scenario involving a nominal diameter of 20 mm.

The obtained results hold significant implications for enhancing our understanding of the impact of high-frequency vibration in the elastic deformation state of materials, as well as its application in SF processes. This insight has the potential to expand the feasibility of interference fits, rectify shortcomings in conventional assembly methods, and lay the groundwork for future technological advancements.

2. MATERIALS AND METHODS

2.1. EXPERIMENTAL SPECIMENS

This experimental study focused on mechanical interference fits, specifically examining the nominal diameter d_N = 20 mm. While previous research on high-frequency oscillation [14, 15] had primarily concentrated on micrometer-level precision in electronic applications, this work aimed to bridge the gap and explore the effects of high-frequency oscillation on larger-scale mechanical fits.

In accordance with DIN 7190-1, which provides calculation and design guidelines for interference fits [16], the chosen machining tolerance for the inner parts (shafts) was p7, while for the outer parts (hubs), it was H7 (as shown in Fig. 1B). Furthermore, the dimensions of other components were selected with linear tolerances in consideration of DIN ISO 2768-1 [17].

As mentioned earlier, previous studies focusing on millimeter-scale nominal diameter values cannot be considered representative cases of symbolic interference assembly due to factors such as the high ratio of contact length to nominal diameter l/d_N [12, 13] and the use of plastic coupling materials [10]. Therefore, this article shifts the focus to S45C steel, a more commonly used material for interference fits.

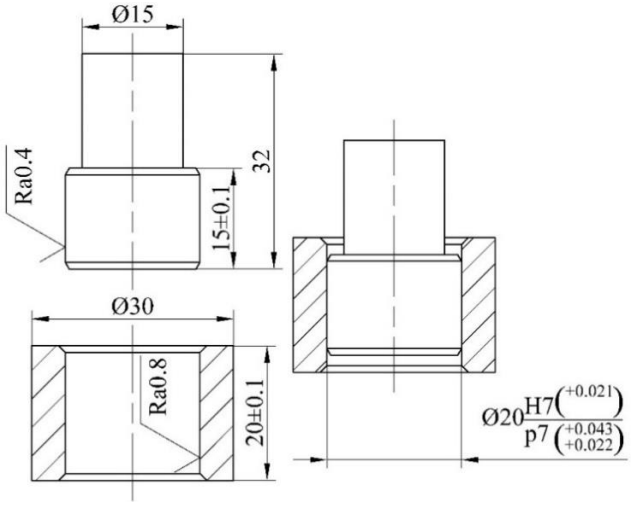

A)

B)

Fig. 1. A) – Experimental specimens schematics, B) – actual workpieces

Regarding JIS G 4051 [18], the mechanical characteristics of S45C grade steel, relevant to this study, are as follows: Young's modulus E = 210 GPa; Poisson's ratio ν = 0.3; yield strength σ = 360 MPa.

First, fifty specimens were chosen, consisting of twenty-five shafts and twenty-five hubs, which were paired based on their diameter differentials. From these pairs, nineteen suitable pairs were selected for the experimental analysis. To ensure the integrity of the specimens between experimental stages, strict measures were taken to store them under controlled conditions, preventing rust formation and contamination.

2.2. INTERFERENCE FIT ASSEMBLY METHODS

2.2.1. CONVENTIONAL PROCEDURES

To begin with, this research focused on the implementation of shrink fits, where the hub specimens were subjected to heat to facilitate the effortless insertion of the shafts. To ensure the precision and accuracy of the assembly, several locating devices were employed to prevent concentricity errors, which have been found to have significant impacts on the load capacity of interference fits [19].

Another conventional process investigated in this study was PF, specifically utilizing a hydraulic compressing machine for axial loading.

In the case of SF, the calculations primarily revolve around the heating temperature and the thermal properties of the specimen's material. This widely adopted approach is rooted in the thermal expansion characteristic of metals, which is well-documented in stand guidelines [16], handbooks, textbooks, and research publications [20, 21]. The relationship can be expressed by the following equation:

$$\Delta_d = \alpha \cdot d_N \cdot \left(t - t_0\right) \tag{1}$$

where Δd is the desired total deformation value (mm); α is the thermal expansion coefficient (1/°C), considering S45C steel, $\alpha = 11.5 \cdot 10^{-6}$ °C^{-1} [18]; d_N is the nominal diameter of the part being heated (mm); t_0 is the part's beginning temperature (°C); t is the required temperature to achieve the suitable deformation (°C).

In the case of interference assembling, where no external forces are applied, it is essential for the desired total deformation Δd to exceed the actual interference value δ_m at a minimum, ensuring a proper interference fit:

$$\Delta_d > \delta_m \tag{2}$$

From Eq. (1) and (2), the relation between the required temperature and the desired interference value is as follow:

$$t > \frac{\delta_m}{\alpha \cdot d_N} + t_0 \tag{3}$$

Once the required heating temperature was determined, the hub specimens were carefully positioned into the PORA muffle furnace (Jin-Bomb Enterprise Co., Ltd., Kaohsiung City, Taiwan) with precise heating parameters, as illustrated in Fig. 2a. Upon the completion of the heating process, the hub specimens were promptly removed from the heating system and proceeded with the joining procedure involving the shaft specimens. As a result of thermal expansion, a controlled micro gap was formed between the shaft and hub, making the insertion of the shafts into the hub effortless. Consequently, the shafts were securely positioned in their desired place, facilitating the final assembly (see the assembling steps in Fig. 2b, 2c, 2d, 2e and the coupled specimens in Fig. 2f).

Another conventional assembly method being investigated is PF, which involves positioning the parts into their desired location through the application of axial loading. The process can range from simply tapping the parts with a rubber hammer to more robust methods such as hydraulic pressing.

In this study, the PF procedures were carried out using hydraulic pressing equipment on the MARUI testing system MIS-225-1-16 (MARUI & Co., Ltd., Osaka, Japan), as depicted in Fig. 3a. This PF setup was also utilized in previous studies [22, 23]. Figure 3b displays the main assembling block, where the specimens were securely held in place by the upper and lower jigs.

The relation between axial force and the interference fit characteristics is broadly discussed as Eq. (4), in which the axial force has to, at least, surpass the sliding frictional limit between surfaces F_f. According to DIN 7190-1 [16]:

$$F_a \geq F_f = \frac{\left[\delta_m - 3 \cdot \left(Ra_s + Ra_h\right)\right] \cdot 10^{-3} \cdot \mu_s \cdot \pi \cdot L}{\frac{1}{E_s} \cdot \left(\frac{d_N{}^2 + d_i{}^2}{d_N{}^2 - d_i{}^2} - \nu_s\right) + \frac{1}{E_h} \cdot \left(\frac{d_o{}^2 + d_N{}^2}{d_o{}^2 - d_N{}^2} + \nu_h\right)} \tag{4}$$

where F_a is the acting axial force (N); μ_s is the static coefficient of friction; L is the length of the contact section between assembly surfaces (mm); E_s and E_h are respectively the shaft and the hub Young's modulus (MPa); v_s and v_h are respectively the shaft and the hub Poisson's ratio; d_i and do are respectively the inner diameter of the shaft and the outer diameter of the hub specimen (mm).

Fig. 2. Shrink-fitting process (SF process) and equipment

Fig. 3. Press-fitting procedures were done with a (a) compression system with (b) the main assembly block

2.2.2. ULTRASONIC OSCILLATION INTEGRATED SHRINK-FITTING

This study aimed to explore the potential benefits of combining ultrasonic oscillation and the conventional interference-fitting process to develop a novel coupling procedure for interference fits. The objective was to enhance the overall workability of the fits and address the limitations of conventional methods.

The basis of this novel process builds upon the analysis of thick-walled cylinders, a well-established problem in elastic theory [1, 24]. The nominal diameter differential between the assembly parts, also known as the interference value, plays a crucial role in determining the strength of the fit. However, in practical manufacturing scenarios, this interference value is not constant. It varies within a statistically studied range, following international guidelines such as DIN 7190-1 [16] or ASME B4.2-1978 (R2020) [25]. Hence, in order to precisely study the effect of ultrasonic oscillation, it is essential to use a series of specimens with the same actual mean interference value $\delta_m = 10$ μm.

Figure 4 demonstrates the novel interference-fitting procedure between a shaft and a hub specimen, having an interference value of δ_{mr}, considering radius differential. Subsequently, the hub specimen is heated to a temperature of t, similar to conventional SF, creating a micro gap between the shaft and hub, as previously mentioned. This facilitates the effortless insertion of the shaft into the hub. Finally, the shrink-fitted joint undergoes oscillation through a high-frequency system.

The principle of the ultrasonic oscillated shrink-fitting (UOSF) process is derived from common ultrasonic applications, such as ultrasonic machining [26] and ultrasonic welding [27], involving longitudinal oscillation. In this study, as depicted in Fig. 5, the experimental setup consisted of an assisting frame holding a pneumatic cylinder, an ultrasonic generator, a transducer, a booster, and an ultrasonic horn. This setup enabled the simultaneous application of axial force to ensure continuous contact between the ultrasonic horn and the joint, along with oscillation on the shrink-fitted joint.

In theory, interference-fitting can be conceptualized as a frictional contact phenomenon occurring between rough surfaces, with the surface asperities playing a predominant role [24]. Therefore, this research can be viewed as a study of frictional contact between rough surfaces under the influence of ultrasonic oscillation.

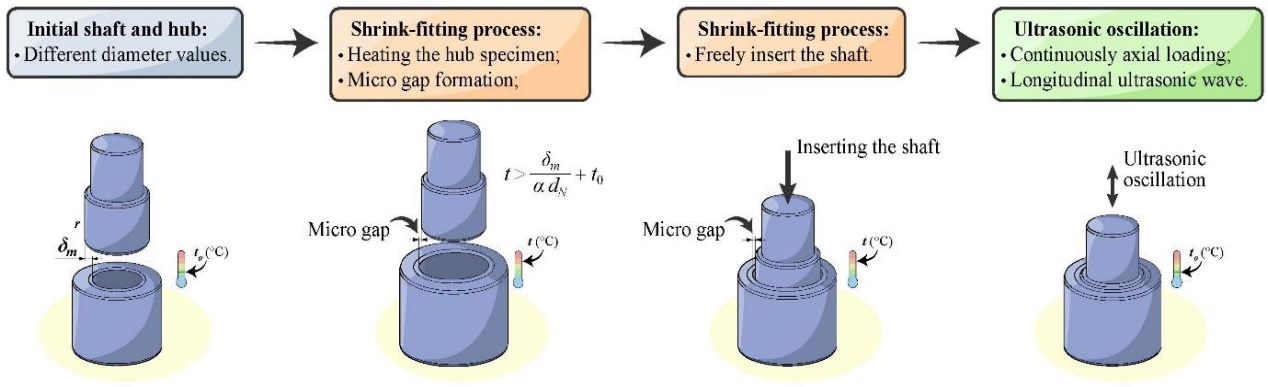

Fig. 4. The simplified procedure of ultrasonic oscillation integrated assembly method

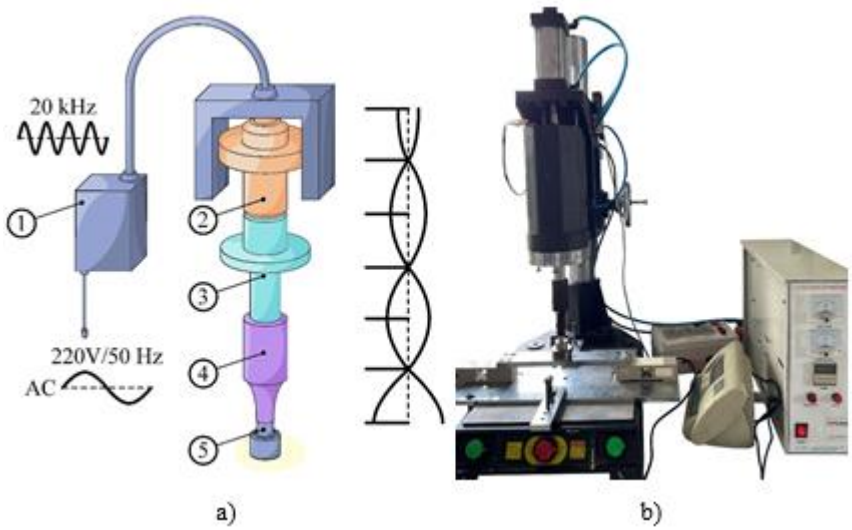

Fig. 5. The ultrasonic oscillating system's (a) principle and (b) experimental setup, including 1–ultrasonic generator, 2–transducer, 3–booster, 4–horn, 5–shrink-fitted joint

A series of experimental works was conducted to determine the optimal parameter set that would yield the highest axial holding load. Building upon this optimal dataset, the remaining ultrasonic oscillated (UO) shrink-fitted specimens were compared to the conventionally assembled ones. This comparison was centered around evaluating the axial holding load and assessing the effects of ultrasonic oscillation.

In existing application studies on ultrasonic oscillation, researchers have placed considerable emphasis on the oscillating time, along with the ultrasonic generating parameters, as crucial inputs. Several preceding studies have explored the oscillating time within 90-second range, yielding promising outcomes. Hence, this research also concentrated on investigating the same period.

Additionally, a crucial parameter under investigation in this study was the generating power P_{uo} of the ultrasonic transducer. It is worth noting that different ultrasonic oscillation system setups can yield diverse outputs even when subjected to the same working inputs. For instance, the relationship between generating power P_{uo} and the oscillating amplitude ξ may not always be linear and can be influenced by several factors, such as the transducer design, materials utilized, and operating frequency. This relationship can be expressed by the following equation (with m and p representing the constants specific to the transducer and the ultrasonic generating system):

$$\xi = m \cdot \left(P_{uo}\right)^{p} \tag{5}$$

This research investigated a range of P_{uo} within 1500 W, corresponding to the working range of the ultrasonic equipment. Additionally, this range of generating power is broadly considered in various research related to ultrasonic applications [28, 29].

To assess the ultrasonic oscillating time t_{uo} and the ultrasonic generating power P_{uo}, a comprehensive examination was carried out using the FCCCD response surface method.

This method incorporates a strategically planned experimental design consisting of four core points, four star points, and one center point. The specific factor levels utilized in the experiment are outline in Table 2.

Table 2. The factor levels

Factor	Symbol		Intervals	Level of factors		
	Uncoded	Coded		-1 (Low)	0 (Middle)	+1 (High)
Ultrasonic oscillating time	t_{uo} (s)	x_1	30	10	40	70
Ultrasonic generating power	P_{uo} (W)	x_2	500	500	1000	1500

In the FCCCD design, the levels of factors are categorized into low, middle, and high levels. For the ultrasonic oscillating time, the range extends from 10 to 70 s, while the ultrasonic generating power ranges from 500 W to 1500 W. These factors can be denoted as ×1 and ×2, respectively, and are evaluated using the three levels of the FCCCD method: low (–1), middle (0), and high (+1).

2.3. PARAMETER INSPECTIONS AND HOLDING FORCE TEST

2.3.1. PARAMETER INSPECTIONS

In order to verify the actual mean interference value of each coupling, the dimensional inspections were carried out on the working surfaces, having the nominal diameter dN = 20 mm. The specimens were placed on comparable jigs to achieve a moderate rigidity for accurate inspections, specifically on the Mitutoyo Beyond-A504 coordinate measuring machine (Mitutoyo Corporation, Sakado, Japan) (see in Fig. 6a). For shafts, the inspection was performed on two evenly allocated cross-sections along the shaft axis, involving contact on twelve points for each section (as shown in Fig. 6b). The process was repeated three times for every shaft specimen and the specimen was rotated an approximately 10° angle between repetitions. For hubs, there were the same inspecting processes with an additional cross-section (presented in Fig. 6c).

Besides diameters, the arithmetic average roughness (Ra) for surface roughness was inspected by Mitutoyo SJ-301 surface profiler (Mitutoyo Corporation, Sakado, Japan) (as presented in Fig. 7a) with Gaussian filter, regarding JIS B 0601 [30] and JIS B 0634 [31] with the profile filter value (also known as cut-off value) λ_c = 0.8 mm and other input conditions as shown in Fig. 7b. The processes were executed twice on six rulings, which are evenly distributed around the circumference, with the specimens being set on a magnetic V-block 6801-1201 (INSIZE Co. Ltd., Suzhou, China) (see Fig. 7c, d). For each inspection, the profiler's stylus was shifted with regard to covering the whole measuring line.

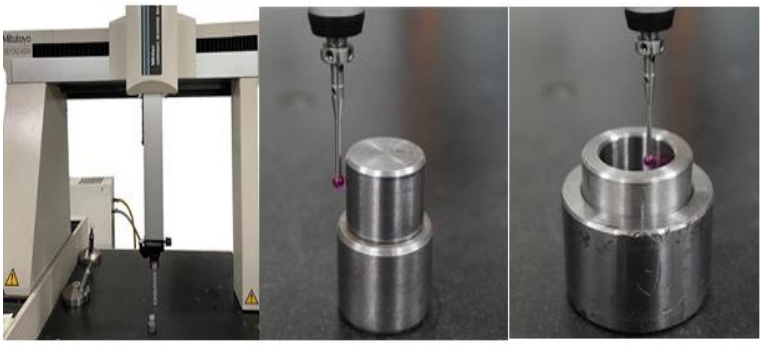

a) b) c)

Fig. 6. Specimen's diameter inspection on (a) Mitutoyo Beyond-A504 coordinate measuring machine for (b) shaft and (c) hub specimens

To meet the requirements of the international tolerance (IT) grade for the shaft and hub specimens, which is IT7 in this case, the commonly employed method is fine grinding. Therefore, following the turning and boring processes, the specimens underwent fine grinding to achieve the desired IT7 tolerance and corresponding surface finish grades. The measured results of these processes are presented in Table 3. The average diameters of specimens fall within the desired tolerance range, ranging from 20.022 mm to 20.043 mm for the shaft specimens with a tolerance of 20p7, and ranging from 20.000 mm to 20.021 mm for the hub specimens with a tolerance of 20H7.

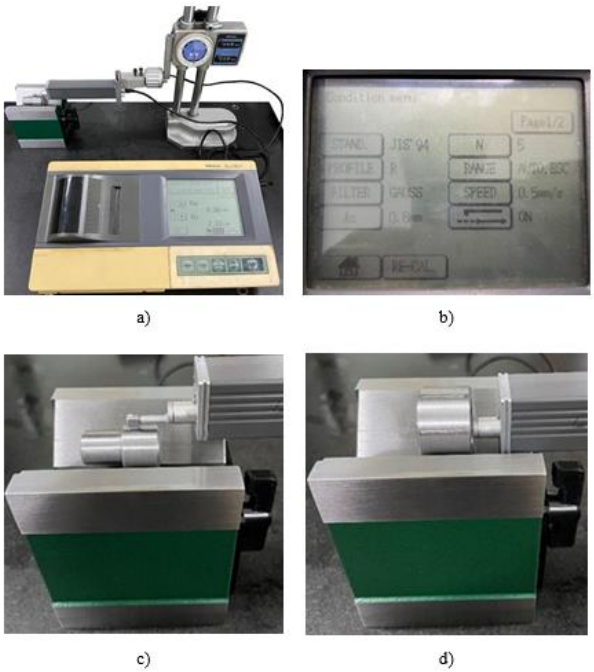

a) b)

c) d)

Fig. 7. Surface roughness inspection on (a) Mitutoyo SJ-301 surface profiler with common (b) input conditions for (c) shaft and (d) hub specimens

As a result of fine grinding processes, based on JIS B 0021 [32], the shaft and hub specimens were finished with the surface roughness values ranging around Ra0.4 and Ra0.8, respectively. More specifically, the measured mean value for the shafts is Ra0.45, while for

the hubs, it is Ra0.96. These surface roughness values are aligned with the desired surface finish grades mentioned earlier.

Table 3. The mean diameter and mean surface roughness value of the specimens after machining

Shaft specimens					
No.	Mean diameter d_N (mm)	Mean surface roughness Ra_s (μm)	No.	Mean diameter d_N (mm)	Mean surface roughness Ra_s (μm)
1	20.023	0.40	11	20.030	0.43
2	20.023	0.39	12	20.031	0.45
3	20.024	0.45	13	20.031	0.48
4	20.024	0.37	14	20.032	0.48
5	20.025	0.41	15	20.032	0.46
6	20.025	0.41	16	20.033	0.48
7	20.026	0.40	17	20.035	0.41
8	20.026	0.43	18	20.035	0.48
9	20.028	0.65	19	20.040	0.55
10	20.028	0.42			
Hub specimens					
No.	Mean diameter d_N (mm)	Mean surface roughness Ra_s (μm)	No.	Mean diameter d_N (mm)	Mean surface roughness Ra_s (μm)
1	20.001	1.13	11	20.017	1.45
2	20.002	1.65	12	20.017	0.76
3	20.002	0.68	13	20.018	1.03
4	20.004	1.28	14	20.018	1.17
5	20.005	0.76	15	20.018	1.21
6	20.007	0.90	16	20.018	0.85
7	20.014	1.12	17	20.019	0.87
8	20.014	0.69	18	20.020	0.73
9	20.016	0.72	19	20.021	0.76
10	20.016	0.59			

2.3.2. HOLDING FORCE TEST

The load capacity of each fit was assessed through a holding force test, employing the same hydraulic system as the conventional PF process depicted in Fig. 3. The assembled samples were securely positioned on the jigs and subjected to a consistent axial load rate of approximately 1 mm/min. The maximum load capacity of each fit was determined by calculating the average load values from the point of complete joint integrity to the point where disconnection begins.

3. EXPERIMENTAL RESULTS AND DISCUSSION

3.1. AXIAL HOLDING LOAD CAPACITY

Initially, this study involved exploratory experimentation to assess the suitability of the ultrasonic oscillation equipment and examine the effects of ultrasonic oscillation in the SF

method. The results showed promising outcomes regarding the benefits of ultrasonic oscillation in SF and confirmed the suitability of the experimental equipment.

Based on these exploratory results, the research delved into investigating the ultrasonic oscillating parameters to identify the optimal setup for achieving the highest holding load. With this goal in mind, the FCCCD experimental design mentioned earlier was employed, involving nine pairs of specimens with a mean interference value of approximately 10 μm. The results of the load capacity tests revealed variations among the different input parameter sets, as summarized in Table 4.

Table 4. FCCCD design for two factors and the holding load result

No.	Symbol			Uncoded levels		Axial holding load
	x_0	x_1	x_2	t_{uo} (s)	P_{uo} (W)	F_a (N)
1	+1	-1	-1	10	500	460
2	+1	+1	-1	70	500	920
3	+1	-1	+1	10	1500	740
4	+1	+1	+1	70	1500	320
5	+1	-1	0	10	1000	920
6	+1	+1	0	70	1000	1050
7	+1	0	-1	40	500	800
8	+1	0	+1	40	1500	600
9	+1	0	0	40	1000	940

The results obtained from the analysis reveal the regression equation that captures the relationship between the axial holding load Fa and the ultrasonic oscillating time t_{uo} and the ultrasonic generating power P_{uo}, as follows:

$$F_a = -851 + 19.61 \cdot t_{uo} + 3.053 \cdot P_{uo} - 0.05 \cdot t_{uo} \cdot t_{uo} - 0.00132 \cdot P_{uo} \cdot P_{uo} - 0.01467 \cdot t_{uo} \cdot P_{uo} \quad (6)$$

To validate the statistical significance and ensure the reliability of the regression model, it was essential to conduct an analysis of variance (ANOVA). Through ANOVA analysis on Minitab software, it was able to assess the contribution and significance of each independent variable. The results, as presented in Table 5, revealed the variance inflation factor (VIF) values of 1, indicating no correlation or multicollinearity among the coefficients in the regression model. These findings provide solid evidence for the validity and reliability of the regression equation.

Table 5. ANOVA analysis

Term	Coefficient	Standard error of the coefficient	T-value	VIF
Constant	1000.0	48.4	20.65	–
t_{uo}	28.3	26.5	1.07	1.00
P_{uo}	-86.7	26.5	-3.27	1.00
$t_{uo} \cdot t_{uo}$	-45.0	45.9	-0.98	1.00
$P_{uo} \cdot P_{uo}$	-330.0	45.9	-7.18	1.00
$P_{uo} \cdot t_{uo}$	-220.0	32.5	-6.77	1.00

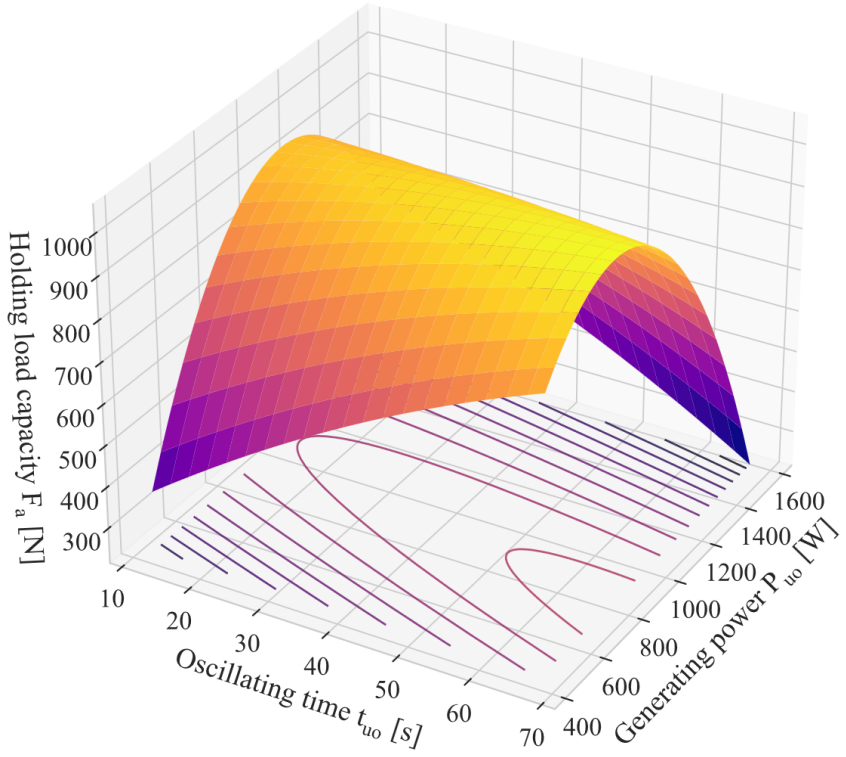

Fig. 8. The axial holding load testing results for FCCCD analysis

The optimal parameters required for achieving the highest axial holding load in the ultrasonic oscillated interference fit were determined. Specifically, these parameters involved setting the ultrasonic oscillating time t_{uo} at a medium level of 70 s and the ultrasonic generating power P_{uo} at a high level of approximately 773 W. With this optimal parameter set, the highest axial holding load limit can theoretically reach the value of approximately 1055 N (as presented in Fig. 9 extracted from Minitab software).

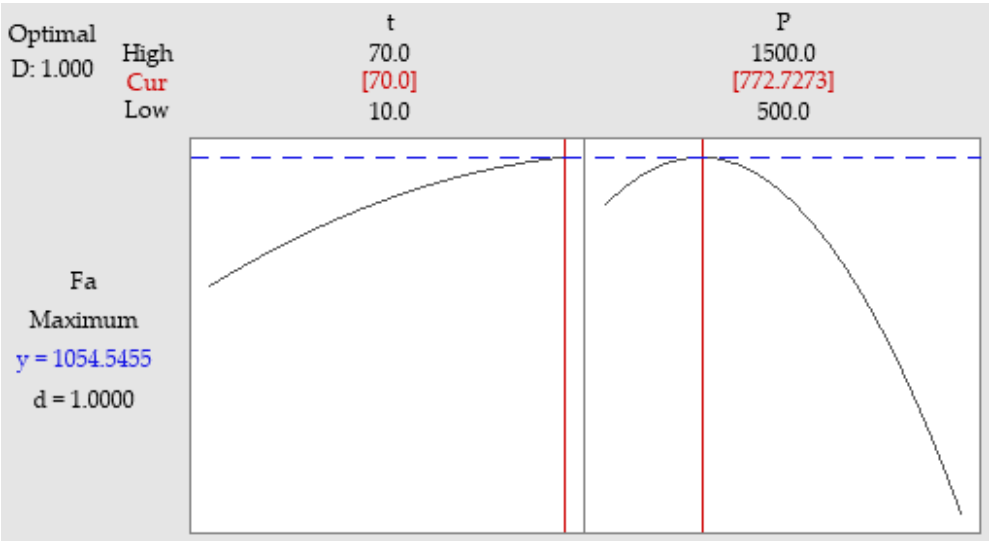

Fig. 9. Response optimization of ultrasonic oscillating parameters

To verify the suitability of the optimal parameters, this study conducted an additional experiment, using the same procedures with the oscillating time of 70 s and a generating power of 750 W. It is worth noting that the choice of 750 W deviated from the optimal result, because it was the closest attainable value with the selected equipment. Evaluating interference-fitted joints featuring a nominal diameter of 20 mm and an interference value of 10 μm, the holding load test affirmed that ultrasonic oscillated shrink fits exhibited the highest load capacity in comparison to conventional methods. These findings further supported the conclusions drawn from the preceding FCCCD analysis. Specifically, the novel assembly process yielded a load threshold of approximately 1040 N, outperforming both PF and normal SF techniques. These methods displayed load capacities of approximately 750 N and 980 N, respectively, as shown in Fig. 10.

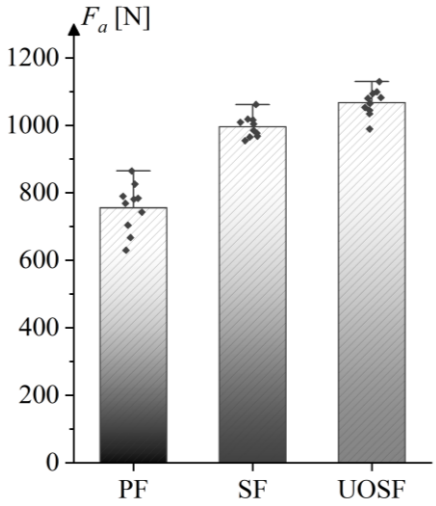

Fig. 10. Holding load test with t_{uo} = 70 s and P_{uo} = 750 W

The observation that the load capacity of the novel method exceeds that of normal PF and SF can be further analysed by investigating the overall effects of ultrasonic oscillation on shrink-fitted joints.

3.2. EFFECTS OF ULTRASONIC OSCILLATION

To conduct an impartial comparison among the assembly methods, it is necessary to disassemble the interference-fitted joints without using any external force. In this research, wire electrical discharge machining (wire EDM) was employed to cut the specimens. This disassembly technique ensures that the working surfaces retain their original conditions as they were during the assembly phase. To achieve this, the joint was oriented with its axis aligned parallel to the wire (see Fig. 11) on the Taizhou DK7725 wire EDM machine (Taizhou Kaiyue Machinery Manufacture Co., Ltd., Jiangsu, China). The cutting process was then initiated and continued until the cut depth reached the critical limit, leading the hub specimen to a failure state that resulted in the disassembly of the parts.

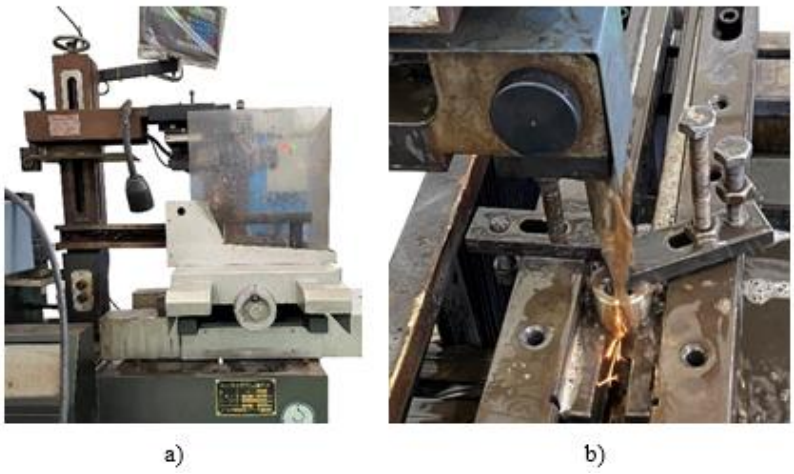

Fig. 11. Disassembling the interference-fitted joints by (a) wire EDM machine with (b) a proportional cutting set up

Similar to the conventional problems, the most noticeable surface behaviour observed involves changes in surface roughness values. When compared with traditional assembly methods, PF consistently displays more pronounced instances of asperities flattening and surface defects than SF. However, when ultrasonic oscillation is integrated into the SF process, there is a considerable enhancement in the surface quality after disassembly (as the results in Fig. 12).

In greater detail, Fig. 12 illustrates a decline in the mean surface roughness value of the press-fitted specimens. Specifically, for the shaft specimen, the roughness value decreased from Ra0.45 to approximately Ra0.32, while the hub's surface roughness experienced a slight drop from Ra0.7 to Ra0.6. A similar pattern was noted in the case of SF, where the hub surface roughness decreased markedly from Ra0.65 to around Ra0.3. In summary, the traditional methods demonstrated an overall reduction in the Ra value of roughly 20% compared to the initial measurement. Conversely, the integrated method contributed to a significant decrease in surface defects after assembly, with the variation accounting for only about 2% of the initial values.

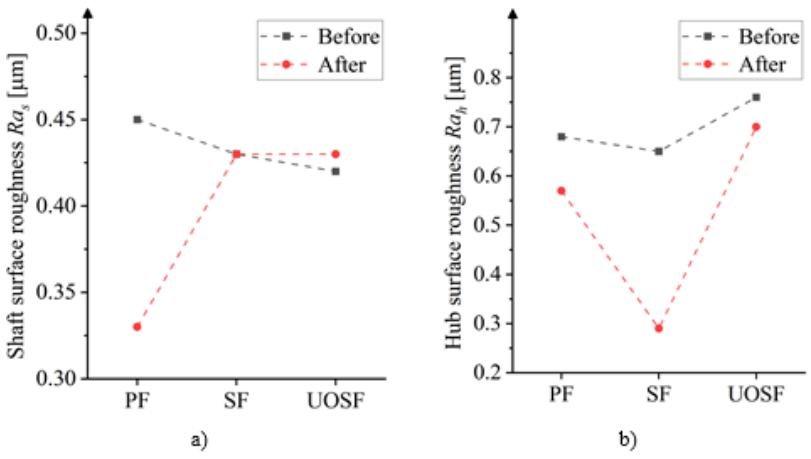

Fig. 12. The general changes of surface roughness value after disassembling of the (a) shaft and (b) hub specimens

While the traditional methods align well with established guidelines regarding surface alterations after assembly, the novel UOSF process yielded promising outcomes, with both Ras and Rah values only exhibiting slight changes. This affirms the potential of ultrasonic oscillation to positively impact surface quality in interference fits.

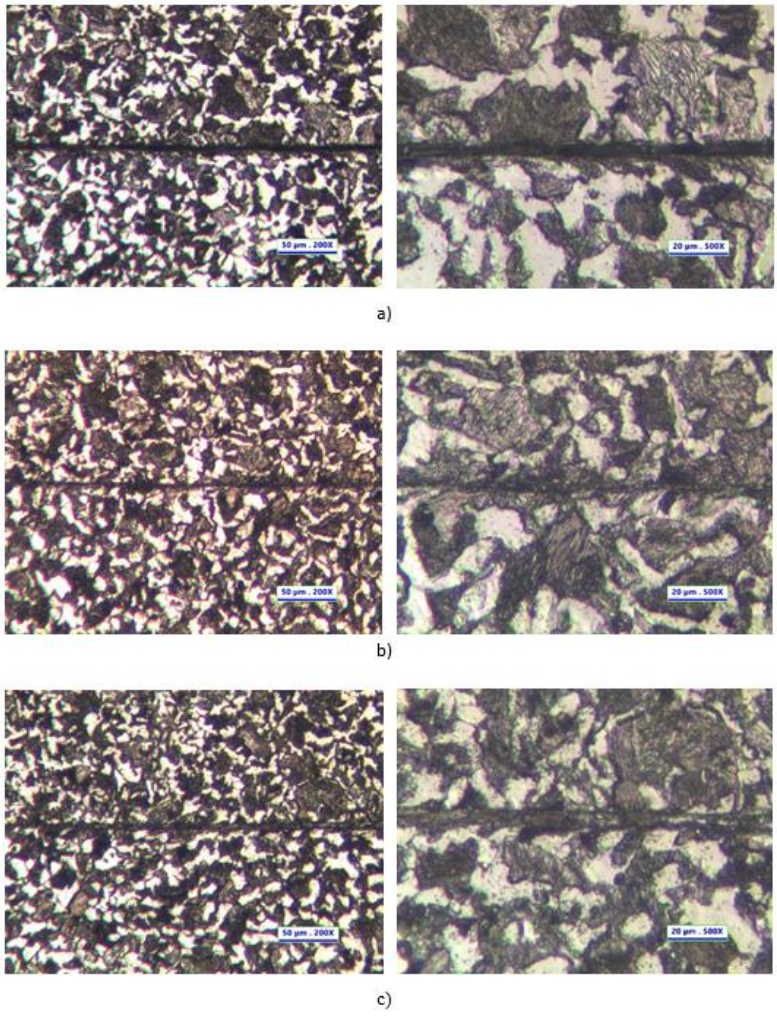

Fig. 13. Interface comparison amongst (a) press-fitting, (b) shrink-fitting, and (c) ultrasonic oscillated shrink-fitting

These outcomes partially explain the holding load testing results, indicating that as working surfaces incurred more severe damage, the interface pressure decreased, thereby weakening the fit. Regarding normal SF, in the assembling stage, the surface asperities do not achieve full contact until the specimens completely cool down, which mitigates most of the flattening and damaging.

Regarding the integrated method, mean surface roughness values experienced a slight reduction compared to conventional SF. This decrease can be attributed to the supplementary oscillation applied in conjunction with the standard SF process. Theoretically, oscillation could potentially induce significant plastic deformations on the working surface, thereby diminishing the fit's holding load. However, empirical evidence unveiled that while deformations did transpire, robust physical adhesions also formed at the interface, establishing strong micro bonds between the shaft and the hub. Essentially, these physical

adhesions outweighed the weakening mechanism triggered by asperities flattening, ultimately boosting the overall load capacity of the fit.

In agreement with the load testing results, press-fitted specimens exhibited the most severe changes in surface roughness values. These changes can be attributed to the continuous interactions between specimen surfaces under high interface pressure, which led to an increased rate of flattening phenomena occurring on these surfaces, consequently reducing the load capacity.

Considering the initial surface roughness levels of the shaft and hub specimens at Ra0.45 and Ra0.96, respectively, with PF, severe damage can be easily spotted on the specimen surface, resulting in a reduction of surface roughness from the initial values of Ra0.45 and Ra0.96 to new values of Ra0.3 and Ra0.6. In the case of conventional SF, where the axial impact present in the PF process is absent, fewer damages are observed at the interface, resulting in slight changes for the shaft specimen and Ra0.3 for the hub specimen. Lastly, in the novel integrated method, there are fewer flattening phenomena than in PF, but slightly more compared to conventional SF, along with the presence of material physical adhesion, resulting in mean roughness values of Ra0.45 for the shaft and Ra0.7 for the hub.

Delving deeper into the physical adhesion phenomena, Fig. 13c presents evidence for the bonding behaviours between the torn material of the shaft specimen and the hub substrate, primarily caused by the material diffusion under ultrasonic oscillation.

Additionally, when compared to other assembly methods, the novel integrated process shows fewer gaps between the shaft and hub surfaces, whereas much more noticeable gaps exist between the assembly parts in the PF and conventional SF cases, as shown in Fig. 13a, 13b.

4. CONCLUSION

Generally, one of the most significant issues in interference-fitting applications is the adverse impact stemming from the assembly procedures, where asperities are prone to being torn away from the surfaces of the assembled parts under high-stress conditions. This problem directly leads to the formation of gaps between the assembled parts and subsequently contributes to various types of joint failures due to surface damage and a decrease in interface stress. The proposed method of integrating high-frequency oscillations after SF has been demonstrated to have beneficial effects on enhancing the diffusion phenomena between the torn asperities and the substrate itself. Specifically, the torn pieces were observed to form new bonds that filled in the gaps, reduced the rate of stress decrease, and improved the overall performance of the shrink-fitted joint. The parameters were analysed to be optimal with 70 seconds of oscillation at a generating power of 773 W, which increased the axial load limit to 1055 N. The rerun experiment confirmed that the UOSF joint's strength could reach as high as 1040 N with the ultrasonic generating power set at 750 W for 70 seconds.

In addition to the strength testing, other aspects were also evaluated to help explain the beneficial effects of the novel assembly procedure. Surface roughness measurements showed that UOSF helped maintain the initial surface condition, as evidenced by the surface

roughness values before and after UOSF. There were only minor changes in the surface conditions, which represent another valuable outcome of material diffusion at the interface, in addition to the formation of new bonds between torn asperities and the substrate surfaces. With the effects of ultrasonic oscillations in shrink-fitted joints, the workability and reliability of interference fits could be significantly increased.

The results were also aligned with previous studies highlighting the lack of research in this field, which complicates the application of interference assemblies in small mechanical systems. Furthermore, this study investigated a different and more common spectrum of oscillation frequency at 20 kHz, contrasting with existing studies that focused on low or extremely high frequencies. In addition to the well-established benefit of ultrasonic oscillation in press-fitting for disassembly, this study confirmed another advantage: enhancing assembly performance, crucial for broader applications and future studies. Therefore, this novel integrated procedure can serve as a critical fabrication technique for newly developed interference-fitted mechanisms used in drones and other small devices, where simple and easy-to-make joints are paramount.

ACKNOWLEDGEMENTS

We acknowledge Ho Chi Minh City University of Technology (HCMUT), VNU-HCM for supporting this study.

REFERENCES

[1] SCHMID S.R., HAMROCK B.J., JACOBSON B., 2014, *Fundamentals of Machine Elements (3rd Ed.)*, CRC Press, New York, https://doi.org/10.1201/b17120.

[2] GROOVER M.P., 2021, *Fundamentals of Modern Manufacturing: Materials, Processes, and Systems*, John Wiley & Sons Singapore Pte Ltd.

[3] RAMAMOORTHY B., RADHAKRISHNAN V., 1994, *A Study of The Surface Deformations in Press and Shrink Fitted Assemblies*, Wears, 173/1–2, 75–83, https://doi.org/10.1016/0043-1648(94)90259-3.

[4] KUMAR S., WU C.S., PADHY G.K., DING W., 2017, *Application of Ultrasonic Vibrations in Welding and Metal Processing: A Status Review*, J. Manuf. Processes, 26, 295–322, https://doi.org/10.1016/j.jmapro.2017.02.027.

[5] MARIUSZ L., PAWEL G., EMILIA B.R., 2023, *The Effect of Contact Compliance of Sliding Pair on Friction Force Reduction at Longitudinal Tangential Vibrations*, Tribology Int., 187, 108701, https://doi.org/10.1016/j/triboint.2023.108701

[6] WANG C.J., LIU Y., GUO B., SHAN D.B., ZHANG B., 2016, *Acoustic Softening And Stress Superposition in Ultrasonic Vibration Assisted Uniaxial Tension of Copper Foil: Experiments and Modelling*, Mater. Des., 112, 246–253, https://doi.org/10.1016/j.matdes.2016.09.042.

[7] SHAO G., LI H., ZHAN M., 2021, *A Review on Ultrasonic-Assisted Forming: Mechanism, Model, and Process*, Chin. J. Mech. Eng., 34/1, https://doi.org/10.1186/s10033-021-00612-0.

[8] DONG S., DAPINO M.J., 2014, *Elastic-Plastic Cube Model for Ultrasonic Friction Reduction Via Poisson's Effect*, Ultrason., 54(1), 343–350, https://doi.org/10.1016/j.ultras.2013.05.011.

[9] HÜYÜK, H., MUSIC, O., KOC, A., KARADOGAN, C., BAYRAM, Ç., 2014, *Analysis of Elastic-Plastic Interference-Fit Joints*, Procedia Eng., 81, 2030–2035, https://doi.org/10.1016/j.proeng.2014.10.276.

[10] MIKOLAINIS, J., BAKSYS, B., 2012, *Experimental Investigation of Interference Fit Connection of Mechanical Components*, J. of Vibroeng., 14/1, 73–78, https://www.extrica.com/article/10551.

[11] LAURENCZY, C., BERLIE, D., JACOT, J., 2014, *Ultrasonic Press–Fitting: A New Assembly Technique*, Precis. Assem. Technol. and Syst., IPAS 2014, IFIP Adv. Inf. and Commun. Technol., 435, 22–29, Springer, Berlin, Heidelberg, https://doi.org/10.1007/978-3-662-45586-9_4.

[12] NIGMETZYANOV R.I., SUNDUKOV S.K., FATYUKHIN D.S., 2017, *Ultrasonic assembly of press-fit joints*, Russian Eng. Res., 37/12, 1044–1047, https://doi.org/10.3103/s1068798x17120139.

[13] DIEUDONNE E., FLORENCE O., JOSEPH N.A., CLAUDE VALERY N.A., ACHILLE N.P., CRICK NELSON Z., 2020, *A Study on the Experimental Investigation of Low Frequency Vibration Wave Assisted Disassembly of Press-Fit Joints*, J. Manuf. Processes, 49, 70–81, https://doi.org/10.1016/j.jmapro.2019.11.014.
[14] HALM C., OTTO A., STARK T., SCHAAF P., 2020, *Ultrasonic Excitation During Press-Fit Joining of Electrical Contacts*, Int. J. Adv. Manuf. Technol., 109/7–8, 2215–2220, https://doi.org/10.1007/s00170-020-05760-6.
[15] HALM C., OTTO A., STARK T., SCHAAF P., 2018, *Enhancing the Retention Force of Press-Fit Connections by Ultrasonic Excitation*, Physica Status Solidi (a), 215/6, 1700598, https://doi.org/10.1002/pssa.201700598.
[16] Deutsches Institut für Normung E.V. (DIN), 2017, *Pressverbände – Teil 1: Berechnungsgrundlagen und Gestaltungsregeln für Zylindrische Pressverbände (DIN 7190-1:2017-02)*, https://dx.doi.org/10.31030/2414563.
[17] Deutsches Institut für Normung E.V. (DIN), 1991, *Allgemeintoleranzen: Toleranzen für Längen und Winkelmaße ohne Einzelne Toleranzeintragung – Identisch Mit ISO 2768-1:1989 (DIN ISO 2768-1:1991-06)*, https://dx.doi.org/10.31030/2458559.
[18] Japanese Standards Association (JSA), 2023, *Carbon Steels for Machine Structural Use (JIS G 4051:2023)*.
[19] RAJ A.P., BHATTI A., DHANISH P.B., 2020, *Combined Effect of Cylindricity, Roundness and Roughness on Axial Load-Carrying Ability of Interference Fits*, Proc. Inst. Mech. Eng., Part J: J. Eng. Tribology, 234/11, 1697–1711, https://doi.org/10.1177/1350650120919883.
[20] WU X., LI C., SUN S., TONG R., LI Q., 2019, *A Study on the Heating Method and Implementation of a Shrink-Fit Tool Holder*, Energies, 12/18, 3416, https://doi.org/10.3390/en12183416.
[21] KROL R., SIEMIATKOWSKI Z., 2019, *The Analysis of Shrink-Fit Connection – The Methods of Heating and the Factors Influencing the Distribution of Residual Stresses*, Heliyon, 5(11)., https://doi.org/10.1016/j.heliyon.2019.e02839.
[22] LOC N.H., PHONG L.V., 2022, *Study of Interference Fit Between Steel and Brass Parts*, EUREKA: Phys. and Eng., 5, 140–149, https://doi.org/10.21303/2461-4262.2022.002524.
[23] LOC N.H., PHONG L.V., 2023, *Effects of Nickel Plating on Interference Fit Between Medium Carbon Steel and Copper–Zinc Alloy Parts*, Met., 13/2, 247, https://doi.org/10.3390/met13020247.
[24] PERSSON B.N., 2022, *Influence of Surface Roughness on Press Fits*, Tribology Lett., 71/1, https://doi.org/10.1007/s11249-022-01688-y.
[25] American Society of Mechanical Engineers (ASME), 2020, *Preferred Metric Limits and Fits (B4.2-1978:R2020)*.
[26] HUANG B., WANG W., XIONG Y., WU X., LIU J., LIU C., WANG D., 2023, *Investigation of Force Modelling in Ultrasonic Vibration-Assisted Drilling SICF/Sic Ceramic Matrix Composites*, J. Manuf. Processes, 96, 21–30, https://doi.org/10.1016/j.jmapro.2023.04.040.
[27] SINGH R.R., SINGH I., KUMAR S.A., 2023, *Ultrasonic Welding of Printed/Molded Sustainable Polymer Specimens with Energy Directors*, Ultrason., 134, 107078, https://doi.org/10.1016/j.ultras.2023.107078.
[28] FARTASHVAND V., ABDULLAH A., SADOUGH VANINI S.A., 2017, *Investigation of Ti-6Al-4V Alloy Acoustic Softening*, Ultrason. Sonochem., 38, 744–749, https://doi.org/10.1016/j.ultsonch.2016.07.007.
[29] NAIK A.S., SURYAWANSHI D., KUMAR M., WAGHMARE R., 2021, *Ultrasonic Treatment: A Cohort Review on Bioactive Compounds, Allergens and Physico-Chemical Properties of Food*, Current Res. Food Sci., 4, 470–477, https://doi.org/10.1016/j.ultsonch.2016.07.007.
[30] Japanese Standards Association (JSA), 2022, *Geometrical Product Specifications (GPS) – Surface Texture: Profile Method – Terms, Definitions and Parameters (JIS B 0601:2022)*.